Hierarchical Multi-Scale Modelling of ROV-Mounted Rolling Brush Systems: From Filament Micro-Dynamics to Full Vehicle Integration

Rishabh Pratap Singh [1], Kishor Kumar Das [1], Prabhat Thakur [1], Bhushan Thool [1], Jagadeesh Kadiyam [1*], Santhakumar Mohan [2]

[1] Indian Institute of Technology Mandi, Himachal Pradesh, India
s23019@students.iitmandi.ac.in, s23020@students.iitmandi.ac.in, s24112@students.iitmandi.ac.in, s23018@students.iitmandi.ac.in
kadiyamjagadeesh@gmail.com
[2] Indian Institute of Technology Palakkad, Kerala, India
santhakumar@iitpkd.ac.in

Abstract. When you use brushes on a remotely operated vehicle (ROV) to clean marine biofouling, it's not just a matter of scrubbing. There are a lot of unknowns in this complicated control problem. The brush's response pressures might easily move the vessel, making it harder to keep it in the right area. Modern models usually simplify brushes to springs or dampers, ignoring the physics behind them. Finite-element models are precise but require substantial computer resources for real-time control. We created a hierarchical modelling approach that links the micro-mechanics of each bristle directly to the full-scale dynamics of the vehicle. We commenced our research by utilising Euler-Bernoulli theory and modal decomposition to define each nylon filament as a flexible cantilever beam. This let us create closed-form equations for the basic response forces. Later, we added a whole brush assembly, including DC motor electromechanics to account for the brush's natural slowing down when loads change, which constant-speed models don't take into consideration. After that, we added this disturbance model to a BlueROV2 simulator with six degrees of freedom. The results show that the brush can create steady forces of up to 221 N (more than twice the vehicle's thrust in some directions) as well as strong resistive torques. Engineers can use this setup to make strong controllers that can handle loads and be used in water before they are put into use.

Keywords: Underwater robotics, ROV dynamics, modal analysis, tool-vehicle interaction, hierarchical modelling, thruster allocation, and marine biofouling.

Nomenclature

Symbol	Definition	Symbol	Definition
Filament & Contact			
L	Filament length	M_r	Modal mass

V. Kumar et al. (eds.), *Proceedings of the International Conference on Advanced Design, Manufacturing, and Sustainable Energy Systems (ICADMSES 2026)*, Atlantis Highlights in Engineering 45,
https://doi.org/10.2991/978-94-6239-750-7_74

d	Filament diameter	N_m	Number of retained modes
E	Young's modulus	β_r	Eigenvalue parameter
ρ	Material density	Δ(t)	Penetration depth
A	Cross-sectional area, $\pi d^2/4$	F_n	Normal contact force
I_zz	Second moment of area, $\pi d^4/64$	F_f	Friction force
y(x,t)	Transverse deflection	k_c, c_c	Contact stiffness and damping
Y_r(x)	Mode shape function	μ_s, μ_c	Static and Coulomb friction coefficients
η_r(t)	Modal coordinate	v_0	Stribeck velocity
ω_r	Natural frequency	k_v	Viscous friction coefficient
ζ_r	Modal damping ratio	v_s	Sliding velocity
N_r(t)	Generalized modal force	α	Filament cant angle
Reaction Forces at Filament Base			
F_y	Transverse shear force	F_z	Axial (normal) reaction force
M_b	Bending moment at base		
Brush Assembly & Motor			
n	Number of filaments	R	Terminal resistance
R_brush	Brush radius	L_a	Armature inductance
θ_i	Angular position of i-th filament	K_e	Back-EMF constant
F_brush	Aggregate brush force	K_t	Torque constant
T_brush	Brush resistive torque	J_m	Rotor inertia
T_load	Motor load torque	B_m	Viscous damping
ω_b	Brush angular velocity	N_g	Gear ratio
I	Motor armature current	ω_m	Motor shaft velocity
V_in	Motor input voltage		
Vehicle Dynamics			
η	Pose vector	τ_control	Control force/moment
ν	Body-fixed velocity vector	τ_disturb	Disturbance force/moment
M	Total mass matrix	B	Thruster allocation matrix
C(ν)	Coriolis matrix	k_T	Thruster force coefficient
D(ν)	Damping matrix	r_tool	Tool mounting position
g(η)	Restoring force vector	m	Vehicle mass
J(η)	Kinematic transformation		

1 Introduction

1.1 Motivation and Problem Context

Marine biofouling, which is the constant buildup of bacteria, algae, and crustaceans on submerged structures, costs marine operations a lot of money. This deposit damages the hull surfaces, which makes the boat use 20–40% more gasoline and costs millions of dollars more each year [1]. Biofouling also causes microbiologically caused corrosion, which is another type of damage [2], makes it easier for invasive species to spread [3], puts offshore installations at risk of becoming unstable [4].

This puts the stability of offshore infrastructure at risk. Cleaning systems that use remotely operated vehicles (ROVs) are a good alternative to traditional dry-docking or chemical methods [5], making it easier to do maintenance while on the job. When the brushes spin around, they create strong reaction pressures that rely on time and make it hard for the vehicle to stay in place. Major problem is created by the way brush filaments, which includes large elastic deformations, sporadic contacts, and changing friction based on speed behave and this reduces the thruster's efficiency and make it difficult to follow a path [6].

A major problem is how closely cleaning tools and moving vehicles are related. External interruptions are frequently seen as separate inputs, in contrast to [7], the forces that come into play during cleaning come from inside the vehicle and depend on its condition, the tools used, and the type of surface being cleaned. This leads to complex feedback processes. Therefore solution to be effective, it is necessary that models cover a range of sizes, fom individual filament interactions to full system reaction s.

1.2 Related Work and Research Gap

The study of modelling and controlling underwater vehicles is a well-known field of research. Fossen [7] builds the typical 6 degree-of-freedom (DOF) rigid body equations, incorporating additional mass, damping and buoyancy effects. A platform with too many actuators, pseudoinverse control allocation [8] and optimisation-driven procedures are important. Resilient methods, including sliding mode control [9], model predictive control [10], and adaptive schemes [11], have showing efficiency against ocean disturbances.

Standard frameworks generally show usually outside pressures because of either limited uncertainty or stable forces [12]. And the research indicates tool-vehicle interactions are limited. Zhang et al. [13] demonstrate a lumped model for hull-climbing cleaners, using the brush as the basic spring-damper system and work good, but it is not very accurate when it comes to physics. Kim and Lee [14] study gives how ROVs behave during water-jet cleaning tests. They saw peak loads of 200 N, but were not able to figure out how to predict these loads.

The Euler-Bernoulli beam theory with modal decomposition is a good middle ground for flexible parts. It is between lumped approximations and full finite-element analysis [15]. Booms on spacecraft, arms on manipulators, and marine risers are all examples of applications. Madanipour and Najafi [16] recently added modal techniques for filaments in underwater cleaning robots, but left out vehicle-level integration and motor dynamics.

There are still big problems: there is no scalable, physics-based model that (1) predicts tool disturbances from first principles; (2) allows tools and vehicles to interact with each other; (3) makes it easier to optimise controllers; and (4) gives the right amount of detail for hardware design choices.

1.3 Contributions

We provide a hierarchical multi-scale simulation system to fill this gap. The main contributions are as follows:

Micro-scale filament dynamics: We show how filament dynamics work by using the first three Euler-Bernoulli modes to illustrate bending. This yields closed-form equations for the three primary reaction components (shear, moment, axial force), integrating geometric nonlinearity and Stribeck friction effects.

Meso-scale actuator-load coupling: We put together a complete brush assembly with concentric filament rows and DC motor electromechanics so that it can work in both directions. The model shows how load torque and back-EMF are related, which, in turn, affects the motor speed and the speed of the contacts.

Macro-scale system integration: We integrate brush disturbance in a full 6-DOF simulation of the BlueROV2 Heavy. This simulation employs an eight-thruster arrangement, pseudoinverse allocation, and cascaded PID loops to maintain the vehicle's position and attitude stability.

Computational Validation Analysis: To ensure physical fidelity, the model is validated using energy balance and force-torque consistency checks with parametric sweeps further quantify the influence of disturbances, offering practical guidance for robust controller tuning. These can be peak forces of up to 221N. Modal analysis and rigid-body dynamics are based on earlier studies. However, our progress comes from putting them together into a single hierarchy that works at different sizes. This method ensures sufficient physical detail for accurate cleaning simulations while preserving the computational speed required for iterative controller development.

1.4 Scope and Limitations

This paper introduces a theoretically verified simulation methodology for internal consistency. Experiments to validate it are designated for subsequent initiatives. The main ideas are: (1) there are no interactions between filaments; (2) hydrodynamic forces on filaments are shown by extra damping terms; (3) cleaning surfaces are locally flat; and (4) biofouling is shown by changed friction coefficients. These kinds of simplifications are common in flexible body analysis and yet make sense from a computational point of view.

1.5 Paper Organisation

Section II describes the full hierarchical modelling method. Section III talks about how each filament moves on a small scale. Section IV explains how the actuator and the load are related. Section V is about fully integrating vehicles. Section VI shows the results of the simulation and the tests of its validity, and Section VII gives the conclusions.

2 Overall Architecture

The ROV-brush setup couples dynamics across scales, from rapid filament vibrations to vehicle-scale maneuvers. Simulating this directly proves too demanding computationally. Instead, we use a hierarchical breakdown for modular, efficient modeling that preserves key interactions.

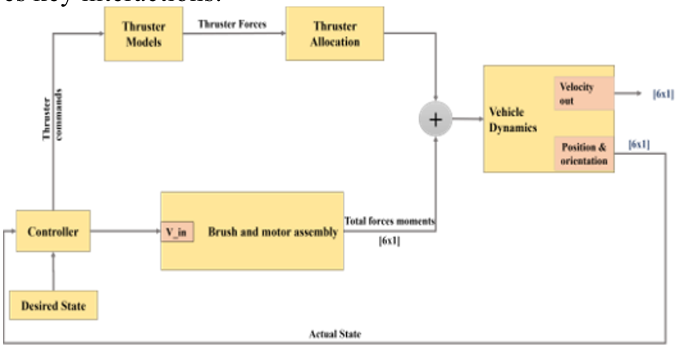

Figure 1. Closed-loop mapping integrating brush motor dynamics with six-dof vehicle control.

Figure 1 illustrates the structure: it links the controller, brush-motor unit, thruster mapping, and 6-DOF vehicle equations with proper feedback paths.

This hierarchy begins with the foundation at the smallest scale.

Micro-model of Single Filament Dynamics: Under modal superposition, this treats each filament as a continuous beam, which gives three response forces components from contact mechanics.

Actuator-Load Assembly (Meso-model): Combines n filaments into a whole brush and uses DC motor calculations to show how load affect speed.

Full Vehicle Integration (System-Model): Using an 8-thruster allocation approach and cascaded PID control for end-to-end mission simulation, it feeds brush disturbances into 6-DOF vehicle motion.

3 Single Filament Micro-Dynamics

The filament-level modelling assumptions are adopted to simplify the filament dynamics while preserving the dominant physical effects:

- Each filament is considered mechanically independent; interactions such as contact, collision, or entanglement between neighbouring filaments are neglected.

- Hydrodynamic effects are approximated using an equivalent viscous damping term, rather than explicitly resolving distributed fluid forces along the filament length.
- The cleaning surface is assumed to be locally planar within the contact region of an individual filament.

The influence of biofouling is incorporated through effective friction coefficients, static friction (μ_s) and Coulomb friction (μ_c), without explicitly modelling discrete fouling organisms.

3.1 Problem Formulation

Consider a single cylindrical filament of length L, diameter d, Young's modulus E, and density ρ. The filament is clamped at the hub ($x = 0$) and undergoes transverse deflection $y(x, t)$ while rolling against a surface with penetration depth $\Delta(t)$. The governing partial differential equation for transverse vibration is:

$$\rho A \frac{\partial^2 y}{\partial t^2} + EI_{zz} \frac{\partial^4 y}{\partial x^4} = f_{\text{ext}}(x, t) \quad \text{.... (1)}$$

where $A = \pi d^2/4$ is the cross-sectional area, $I_{zz} = \pi d^4/64$ is the second moment of area, and f_{ext} represents distributed external forces from contact and friction.

3.2 Modal Decomposition

To avoid the computational cost of direct PDE solution, we employ modal analysis, expressing the solution as a sum of mode shapes:

$$y(x, t) = \sum_{r=1}^{N_m} Y_r(x) \eta_r(t) \quad \text{....(2)}$$

where $Y_r(x)$ are the orthogonal cantilever beam mode shapes given by:

$$Y_r(x) = \cosh(\beta_r x) - \cos(\beta_r x) - \sigma_r[\sinh(\beta_r x) - \sin(\beta_r x)] \quad \text{... (3)}$$

Here, $\sigma_r = (\sinh\beta_r L - \sin\beta_r L)/(\cosh\beta_r L + \cos\beta_r L)$, and β_r satisfies $\cos(\beta_r L)\cosh(\beta_r L) = -1$.

The modal coordinates $\eta_r(t)$ are governed by uncoupled ordinary differential equations:

$$\ddot{\eta}_r + 2\zeta_r \omega_r \dot{\eta}_r + \omega_r^2 \eta_r = N_r(t) \quad \text{....(4)}$$

where $\omega_r = \beta_r^2 \sqrt{EI_{zz}/(\rho A)}$ is the r-th natural frequency, ζ_r is the modal damping ratio, and $N_r(t)$ is the generalised force:

$$N_r(t) = \frac{1}{M_r} \int_0^L f_{\text{ext}}(x, t) Y_r(x) dx \quad \text{....(5)}$$

with modal mass $M_r = \rho A \int_0^L Y_r^2(x) dx$.

3.3 Contact Mechanics and External Forces

External forces, consisting of normal contact and tangential friction, are modelled as concentrated loads near the filament tip:

$$f_{\text{ext}}(x,t) = \left[F_n(t)\hat{\mathbf{n}} + F_f(t)\hat{\mathbf{t}}\right]\delta(x - x_{\text{contact}}) \quad \ldots.(6)$$

Normal Force: We apply Hertzian contact theory, linearised for small deflections:

$$F_n = k_c\Delta^{3/2} + c_c\dot{\Delta} \quad \ldots(7)$$

where k_c and c_c are contact stiffness and damping coefficients, respectively. The penetration depth is defined as:

$$\Delta(t) = R_{\text{brush}} - [R_{\text{brush}} - L\cos\alpha - y(L,t)] \quad \ldots.(8)$$

with α being the filament angle relative to the radial direction.

Friction Force: A Stribeck friction model used to capture static, Coulomb, and viscous regimes:

$$F_f = F_n\left[\mu_c + (\mu_s - \mu_c)e^{-(v_s/v_0)^2} + k_v v_s\right]\text{sgn}(v_s) \quad \ldots(9)$$

where μ_s and μ_c are static and Coulomb friction coefficients, v_0 is Stribeck velocity, k_v is viscous coefficient, and v_s is sliding velocity:

$$v_s = \omega_b R_{\text{brush}} - v_{\text{ROV}} - \dot{y}(L,t) \quad \ldots(10)$$

3.4 Reaction Force Derivation

Reaction forces at the filament base are derived from equilibrium conditions:

Transverse Shear Force F_y:

$$F_y(0,t) = EI_{zz}\frac{\partial^3 y}{\partial x^3}|_{x=0} = EI_{zz}\sum_{r=1}^{N_m} Y_r'''(0)\eta_r(t) \quad \ldots(11)$$

Bending Moment M_b:

$$M_b(0,t) = EI_{zz}\frac{\partial^2 y}{\partial x^2}|_{x=0} = EI_{zz}\sum_{r=1}^{N_m} Y_r''(0)\eta_r(t) \quad \ldots(12)$$

Axial Force F_z: Using the tip angle $\theta_{\text{tip}} \approx \sum Y_r'(L)\eta_r(t)$:

$$F_z \approx F_n\theta_{\text{tip}} - F_f \quad \ldots(13)$$

3.5 Physical Interpretation of Modal Parameters

Eigenvalues and Natural Frequencies: The eigenvalues λ_r determine the spatial frequency of each mode, related to natural frequencies by $\omega_r = \lambda_r^2\sqrt{EI_{zz}/(\rho A)}$. Table 1 lists the first three modal parameters.

Table 1. Modal Parameters for Single Filament

Mode	λ_r	ω_r (rad/s)	Physical Meaning
1	1.875	47.2	Fundamental bending
2	4.694	132.1	Second harmonic
3	7.855	294.3	Third harmonic

The fundamental mode ($\lambda_1 = 1.875$) has one antinode at the tip and is the main part of the response, taking up around 78% of the kinetic energy. It can track surfaces well since its frequency (47 Hz) is lower than the blade-pass frequency (125 Hz).

Higher modes ($r = 2{,}3$) provide more complex variations patterns, as shown in figure 2 by the interior nodes. These modes are mainly excited during impact transients, such as hitting hard fouling. Even though they break down quickly, repetitive stimulation can make you worries.

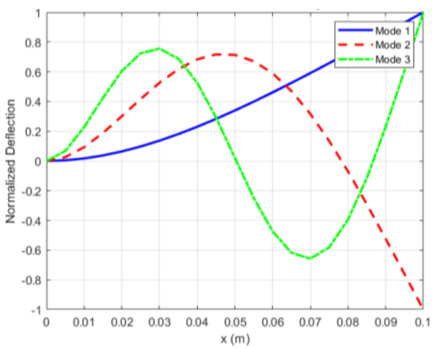

Figure. 2. First three bending mode shapes of the filament

Connection to Existing Research: This study builds on the work of Madanipour and Najafi. We added centrifugal stiffness using the phrase $\rho A_c \omega^2 (r_A + x\sin\phi)\cos\phi$, which significantly increases effective stiffness and natural frequencies, stopping instability at low frequencies.

3.6 Numerical Implementation

The modal ODEs are solved using a 4th order Runge-Kutta scheme with adaptive time stepping (10^{-4} to 10^{-3} s). Retaining $N_m = 3$ Mode's capture over 95% of the total kinetic energy for the relevant frequency range (0-500 Hz).

4 Coupled Actuator-Load Model

4.1 4.1 Brush Assembly Aggregation

The complete brush comprises n filaments. Total reaction forces are obtained by summing the contributions of n parallel filament instances, phase-shifted by $\theta_i = 2\pi(i-1)/n$:

$$\mathbf{F}_{\text{brush}} = \sum_{i=1}^{n} \mathbf{F}_{\text{react},i}(\theta_i) \quad \ldots(14)$$

The aggregate resistive torque about the brush axis, denoted T_brush to distinguish it from the filament bending moment M_b, is:

$$T_{\text{brush}} = R_{\text{brush}} \sum_{i=1}^{n} F_{y,i} \cos(\theta_i + \omega_b t) \quad \ldots(15)$$

4.2 DC Motor Electromechanics

The actuator is modelled as a permanent magnet DC motor with a planetary gearbox, governed by:

Electrical:

$$L_a \frac{dI}{dt} = V_{\text{in}} - RI - K_e \omega_m \quad \ldots(16)$$

Mechanical:

$$J_m \frac{d\omega_m}{dt} = K_t I - B_m \omega_m - \frac{T_{\text{brush}}}{N_g} \quad \ldots(17)$$

where parameters include armature current I, input voltage V_{in}, back-EMF constant K_e, torque constant K_t, rotor inertia J_m, and gear ratio N_g.

4.3 Bidirectional Coupling

A key innovation of this framework is the bidirectional coupling: T_{brush} directly retards motor speed via Eq. (21), which subsequently alters filament sliding velocity via Eq. (12). This feedback loop correctly represents the motor slowdown that happens when the load is heavy, which is an important effect that is typically overlooked in models with constant speed.

5 Full Vehicle Integration

5.1 6-DOF Vehicle Dynamics

We employ Fossen's standard formulation for marine craft. The vehicle state is defined by pose $\boldsymbol{\eta} = [x, y, z, \phi, \theta, \psi]^T$ and body-fixed velocities $\boldsymbol{\nu} = [u, v, w, p, q, r]^T$. The equations of motion are:

$$\dot{\boldsymbol{\eta}} = \mathbf{J}(\boldsymbol{\eta})\boldsymbol{\nu} \quad \ldots(18)$$

$$\mathbf{M}\dot{\boldsymbol{\nu}} + \mathbf{C}(\boldsymbol{\nu})\boldsymbol{\nu} + \mathbf{D}(\boldsymbol{\nu})\boldsymbol{\nu} + \mathbf{g}(\boldsymbol{\eta}) = \boldsymbol{\tau}_{\text{control}} + \boldsymbol{\tau}_{\text{disturb}} \quad \ldots(19)$$

Here, $\mathbf{M} = \mathbf{M}_{RB} + \mathbf{M}_A$ is the total mass matrix, $\mathbf{C}(\boldsymbol{\nu})$ is the Coriolis-centripetal terms, and $\mathbf{D}(\boldsymbol{\nu})$ is the linear and quadratic hydrodynamic damping. Restoring forces $\mathbf{g}(\boldsymbol{\eta})$ take into consideration both buoyancy and gravity.

5.2 8-Thruster Vectored Configuration

The BlueROV2 Heavy utilises 8 T200 thrusters in a vectored configuration. The thrust force F_i is related to the control signal u_i by $F_i = k_T \mathrm{sgn}(u_i) u_i^2$. The allocation matrix $\mathbf{B} \in \mathbb{R}^{6\times 8}$ maps these forces to body-frame generalised forces:

$$\boldsymbol{\tau}_{\text{control}} = \mathbf{B}\mathbf{F}_T \quad \ldots(20)$$

5.3 Disturbance Integration

The brush reaction forces are turned into a disturbance torque vector and applied to the vehicle body frame:

$$\boldsymbol{\tau}_{\text{disturb}} = \begin{bmatrix} \mathbf{R}_{\text{tool}}^{\text{body}} \mathbf{F}_{\text{brush}} \\ \mathbf{r}_{\text{tool}} \times (\mathbf{R}_{\text{tool}}^{\text{body}} \mathbf{F}_{\text{brush}}) + \mathbf{M}_{\text{brush}} \end{bmatrix} \quad \ldots(21)$$

where $\mathbf{r}_{\text{tool}}$ denotes the tool mounting position.

6 Simulation Results and Validation

We implemented the hierarchical framework in MATLAB/Simulink for a realistic hull-cleaning scenario. The analysis below confirms the model's internal consistency and reveals the intricate tool-vehicle interactions.

6.1 Simulation Parameters and Setup

Table 2 summarises the physical parameters used in the simulation, chosen to represent a commercial-grade observation-class ROV (BlueROV2 Heavy) equipped with a medium-duty nylon cleaning brush. These parameters are derived from component datasheets and standard material properties to ensure physical realism.

TABLE 2. Simulation Physical Parameters

Parameter	Value	Description
Filament Properties		
L	0.08 m	Filament length
d	0.8 mm	Filament diameter
E	2.5 GPa	Young's modulus (nylon-6)
ρ	1140 kg/m^3	Material density
Brush Assembly		
n	50	Number of filaments

Parameter	Value	Description
R_{brush}	0.15 m	Brush radius
μ_s/μ_c	0.6/0.4	Friction coefficients
Motor Parameters		
R	0.08 Ω	Terminal resistance
K_t	0.016 N-m/A	Torque constant
N_g	5.22	Gear ratio
Vehicle Properties		
m	11.5 kg	Vehicle mass
$B - W$	0.3 N	Net buoyancy

6.2 Basis for Parameter Selection and Sensitivity

Friction coefficients. μ_s = 0.6, μ_c = 0.4 from published tribological data for nylon-6 on wet painted steel. ±20% perturbation shifts F_y by ±18% and T_brush proportionally; F_z varies by <5%.

Modal damping ratios. ζ_r = 0.02 for all modes, from measured values for slender nylon in water. Increasing ζ_r from 0.01 to 0.05 attenuates peak transients by up to 30% but changes steady-state by <4%.

Modal truncation (N_m = 3). Three modes capture >95% of kinetic energy. A fourth mode changes steady-state forces by <0.8%, confirming convergence.

6.3 Internal Consistency Validation

For any multi-scale model to work well, energy and momentum must be conserved at all levels of the hierarchy. We validated the force-torque relationship between the micro-scale filament model and the meso-scale brush assembly. Total resistive torque, in theory T_brush should equal to the product of the tangential shear force Fy and the moment arm R_brush.

The simulation yielded a stable resistive torque of T_brush =-16.63 N-m and an aggregate tangential force of Fy = -110.9 N. The 0.15% relative inaccuracy shows that our method of combining data is accurate and that forces move well from the tips of the filaments to the motor shafts.

6.4 Analysis of Tool-Induced Disturbances

The system shows analyses under a nominal cleaning scenario: forward vehicle velocity $v_{\text{ROV}} = 0.05$ m/s, brush penetration depth $\Delta = 5$ mm, and motor input voltage $V_{\text{in}} = 12$ V. Table 3 shows the steady-state data, which indicate strong tool-vehicle coupling effects.

Normal contact force (F_z) of filament, shows the transient impact with phase and the settling to a mean load of -221 N as shown in figure 3.

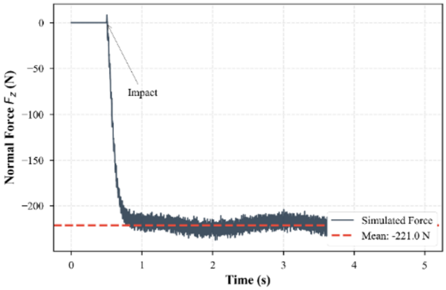

Figure. 3. Normal Contact Force (F_z)

Brush resistive torque (T_{brush})Opposing the motor rotation, stabilizing at approximately -16.63 N-m under load as shown in figure 4.

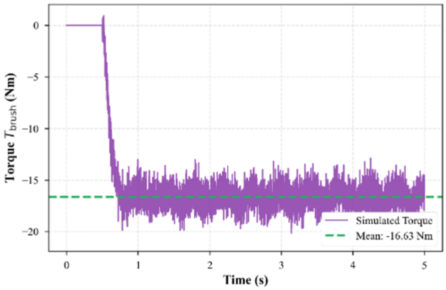

Figure. 4. Brush Resistive Torque T_brush

TABLE 3. Steady-State Simulation Results

Output	Value	Unit	Physical Interpretation
F_z	-221.7	N	Normal contact load
T_{brush}	-16.63	N-m	Brush resistive torque on vehicle yaw/roll
F_y	-110.9	N	Reaction force opposing brush rotation
ω_b	15.7	rad/s	Loaded brush speed (approx. 150 RPM)
q	-0.17	rad/s	Induced pitch rate (≈ 10°/s)

Normal Force Dominance: The normal contact force (N) is the result. The load is around 24 times the vehicle's net buoyancy. This level of disturbance significantly exceeds usual environmental stresses, such as currents or tether drag. This means that keeping the station in place while cleaning requires both stabilisation and force control. If you don't use active thrust adjustment, the vehicle will separate from the hull and lose contact.

Cross-Coupling Effects: The cleaning tool not being in the right place means that translation and rotation depend on each other a lot. The steady-state pitch rate of rad/s shows that the resistive torque (N-m) and normal force make a big pitch moment. This means that a simple PID controller that treats complicated force dynamics as unmodelled disturbances is not likely to stay in the cleaning position.

Actuator-Load Feedback: The simulation clearly demonstrates that two-way communication can occur. The motor experiences resistive torque loading when the brush makes contact with the surface. The back-EMF decreases, maintaining the brush speed at 15.7 radians per second. The ability to self-regulate is very important. A simple model that keeps a constant speed may overestimate frictional forces when stiction happens, which can lead to wrong control inputs.

The motor speed response shows that the speed drops from no-load speed (20 rad/s) to loaded condition (15.7 rad/s) because of back-EMF feedback. The brush reaction torque affects the vehicle pitch rate, which makes it tend to pitch up or down depending on how far away the mounting point is.

7 Conclusion

This study outlines a precise, hierarchical, multi-scale simulation framework for remotely operated vehicle (ROV) mounted hull cleaning systems. We have developed a forecasting tool that transcends Bernoulli beam microdynamics, electromechanical actuator connection, and six degrees of freedom vehicle rigid-body mechanics. The main findings of this study are:

- Spring-damper models do not accurately represent the complex, frequency-dependent characteristics of brush mechanics, especially the mode-dependent stiffening and Stribeck friction behaviours crucial for precise estimation of load.
- The reciprocal interaction of brush load and motor dynamics is essential for achieving balance, but it is often overlooked in contemporary research.
- The shown amplitude and cross-coupling of response forces make a strong case for using model-based control systems instead of traditional PID loops. Examples of these systems are hybrid position/force control and feedforward disturbance rejection.

We plan to test the framework in a fully equipped testbed and create nonlinear control algorithms that use the disturbance model to keep the station stable in the future.

Acknowledgment. Partially supported by the Indian Institute of Technology Mandi seed grant, India (\# IITM/SG/JKD/110), IIT Guwahati Technology Innovation and Development Foundation (TIDF), India, (\# TIH/TD/0213), Deep Ocean Mission, Ministry of Earth Sciences, India (\# MoES/ PAM/DOM/196/2023 (E15710)), and the Anusandhan National Research Foundation

Prime Minister Early Career Research Grant (ANRF-PMECRG)India(\#ANRF/ECRG/2024/002069/ENS).

Disclosure of Interests. The authors have no competing interests to declare that are relevant to the content of this article.

References

1. M. P. Schultz, J. A. Bendick, E. R. Holm, and W. M. Hertel, "Economic impact of biofouling on a naval surface ship," *Biofouling*, vol. 27, no. 1, pp. 87–98, 2011.
2. I. B. Beech and J. Sunner, "Recent advances in the study of biocorrosion: An overview," *Revista de Microbiologia*, vol. 35, no. 3, pp. 177–190, 2004.
3. J. L. Molnar, R. L. Gamboa, C. Revenga, and M. D. Spalding, "Assessing the global threat of invasive species to marine biodiversity," *Frontiers in Ecology and the Envi-roN-ment*, vol. 6, no. 9, pp. 485–492, 2008.
4. I. Fitridge, T. Dempster, J. Guenther, and R. de Nys, "The impact and control of biofouling in marine aquaculture: A review," *Biofouling*, vol. 28, no. 7, pp. 649–669, 2012.
5. D. M. Yebra, S. Kiil, and K. Dam-Johansen, "Antifouling technology—Past, present and future steps towards efficient and enviroN-mentally friendly antifouling coatings," *Progress in Organic Coatings*, vol. 50, no. 2, pp. 75–104, 2004.
6. H. Olsson, K. J. Åström, C. Canudas de Wit, M. Gäfvert, and P. Lischinsky, "A new model for control of systems with friction," *IEEE Transactions on Automatic Control*, vol. 43, no. 3, pp. 419–425, 1998.
7. T. I. Fossen, *Handbook of Marine Craft Hydrodynamics and Motion Control*. Chichester, U.K.: John Wiley & Sons, 2011.
8. T. A. Johansen and T. I. Fossen, "Control allocation - A survey," *Automatica*, vol. 49, no. 5, pp. 1087–1103, 2013.
9. T. Salgado-Jimenez, B. Jouvencel, and E. Campos, "Adaptive sliding mode control of autonomous underwater vehicles with uncertain dynamics," *Ocean Engineering*, vol. 179, pp. 211–219, 2019.
10. C. Shen, Y. Shi, and B. Buckham, "Trajectory tracking control of an autonomous underwater vehicle using Lyapunov-based model predictive control," *IEEE Transactions on Industrial Electronics*, vol. 65, no. 7, pp. 5796–5805, 2018.
11. W. M. Bessa, M. S. Dutra, and E. Kreuzer, "Adaptive fuzzy sliding mode control for autonomous underwater vehicles," *Robotics and Autonomous Systems*, vol. 58, no. 1, pp. 16–26, 2010.
12. G. Antonelli, *Underwater Robots: Motion and Force Control of Vehicle-Manipulator Systems*, vol. 96, Springer Tracts in Advanced Robotics. Berlin, Germany: Springer, 2014.
13. W. Zhang, N. Wang, Y. Li, and G. Chen, "Modeling and simulation of a hull cleaning robot with brush-surface interaction," *IEEE Access*, vol. 7, pp. 168897–168908, 2019.

14. J. Kim, P. Lee, and H.-S. Choi, "Dynamic analysis and control of an underwater cleaning robot for ship hull maintenance," *Ocean Engineering*, vol. 213, p. 107765, 2020.
15. L. Meirovitch, *Fundamentals of Vibrations*. New York, NY, USA: McGraw-Hill, 2001.
16. V. Madanipour and F. Najafi, "Modal analysis of underwater hull cleaning robot considering enviroN-mental interaction," *Ocean Engineering*, vol. 273, p. 113821, 2023